Progress In Electromagnetics Research C, Vol. 67, 97–105, 2016

Triple-Band Dual-Polarized Hybrid Cylindrical Dielectric Resonator Antenna with Hybrid Modes Excitation

Anand Sharma and Ravi K. Gangwar*

Abstract—In this article, a dual-polarized hybrid cylindrical dielectric resonator antenna (CDRA) is studied. A ring-shaped patch along with an inverted L-strip is used to excite two different hybrid modes ($HE_{11\delta}$ and $HE_{12\delta}$-like mode) in CDRA. $HE_{12\delta}$ mode in CDRA is very advantageous in terms of gain and radiation characteristics. The proposed antenna design shows triple-band characteristics, i.e., 1.88–2.06 GHz, 2.29–2.58 GHz and 2.9–3.93 GHz with the fractional bandwidth of 9.13%, 11.9% and 30.16%, respectively. Due to inverted L-strip, it shows circular polarization characteristics within the frequency range 3.3–3.55 GHz (AR $<$ 3 dB). The simulated results are practically verified by using archetype of proposed antenna structure. The proposed antenna design is applicable to WLAN (2.4 GHz) and WiMAX (2.5/3.5 GHz) applications.

1. INTRODUCTION

Due to rapid growth in wireless communication, the research on low profile, multiband and dual-polarized antennas is extremely focused. Different types of antennas are available to fulfill all these requirements, such as microstrip antenna, slot antenna, and dielectric resonator antenna (DRA). Out of these antennas, DRA is one of the most noticeable radiators due to its integral potentials such as no metallic loss and high radiation efficiency [1].

In order to develop multiband characteristics in DRA, several techniques have been developed such as higher order mode generation (HEM_{111} and HEM_{113} mode) in cylinder-shaped DRA [2]. Different shapes of DRA have also been studied to obtain multiband characteristics such as pentagon, stair rectangular DRA [3, 4]. There are various higher order modes such as $HE_{21\delta}$ mode which is quite easily generated in CDRA due to its low quality factor. These modes are not advantageous in the case of antenna because it affects the radiation characteristics of other fundamental modes. Similarly, it is not easy to generate higher order modes (which is useful in the case of antenna) with the help of a simple feed structure [5, 6]. In order to avoid these difficulties, the concept of hybrid DRA comes into existence, which represents combination of DRA with other resonating structures [7, 8]. Similarly, Khalily et al. presented a hybrid CDRA (split half CDRA with fork shape monopole) for multiband applications [9]. Cylindrical DRA along with parasitic slots on ground plane was proposed by Sharma and Gangwar [10]. Recently, dual-polarized antennas are the most favorable topic of the researchers due to their several advantages such as orientation insensitive, getting more information by radar from targets, etc. In order to achieve dual polarizations along with multiband characteristics, some of the studies have been carried out by different researchers such as aperture fed grooved modified RDRA (Rectangular Dielectric resonator antenna), probe-fed semi eccentricannular shaped DRA and metal covered CDRA [11–13].

In this article, we concentrate our study to achieve multiband and dual-polarization characteristics in hybrid CDRA (combination of CDRA and ring shape patch along with inverted L-strip). The preliminary phase of the present article is mainly focused to attain multiband characteristics with the help of hybrid nature of the proposed antenna along with higher order mode excitation in CDRA.

Received 9 June 2016, Accepted 3 September 2016, Scheduled 17 September 2016
* Corresponding author: Ravi Kumar Gangwar (ravi.gangwar.ece07@itbhu.ac.in).
The authors are with the Department of Electronics Engineering, Indian School of Mines, Dhanbad, Jharkhand 826004, India.

After that, we will move the proposed antenna analysis towards dual-polarization characteristics with the help of an inverted L-strip. Recently, the generation of $HE_{12\delta}$ mode in CDRA is mainly focused by different researchers, due to its higher gain and broadside radiation properties. That is why the generation of $HE_{12\delta}$-like mode with the help of modified feed is another important feature of the proposed antenna. The proposed hybrid antenna design is suitable for different wireless applications such as WLAN (2.4 GHz) and WiMAX (2.6/3.5 GHz). The present article is organized as follows: antenna design with mathematical investigation, parametric analysis, experimental results and conclusion are described in Sections-2, 3, 4 and 5, respectively.

2. ANTENNA DESIGN AND MATHEMATICAL ANALYSIS

The 2D view along with feeding structure and panoramic view of proposed antenna are shown in Fig. 1(a) and Fig. 1(b), respectively. In the proposed antenna design, cylindrical shape DRA (Al_2O_3 ($\varepsilon_{\text{Alumina}} = 9.8$, $\tan\delta = 0.002$ is placed over an FR4 substrate ($\varepsilon_r = 4.4$, $\tan\delta = 0.02$). Fig. 2(a) and Fig. 2(b) show the prototype of the proposed antenna with top and bottom views, respectively. Optimum dimensions of different antenna parameters are specified in Table 1.

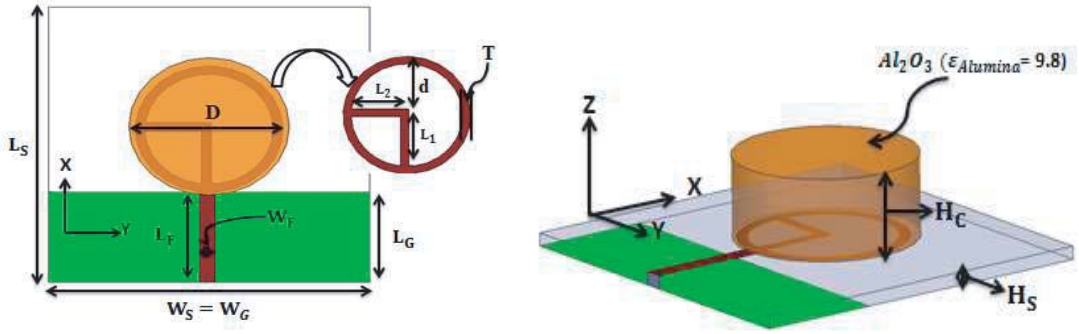

(a) (b)

Figure 1. Schematic diagram of proposed antenna structure. (a) 2D view with feeding structure. (b) Panoramic view.

(a) (b)

Figure 2. Archetype of proposed antenna Structure. (a) Top view. (b) Bottom view.

The resonant frequency of $HE_{11\delta}$ mode in cylindrical shape DRA is given as follows [14]:

$$f_r = \frac{6.321c}{2\pi d\sqrt{\varepsilon_{r,eff}+2}}\left[0.27 + 0.36\left(\frac{d}{2H_{eff}}\right) + 0.02\left(\frac{d}{2H_{eff}}\right)\right] \quad (1)$$

where, c is the velocity of light, $d = D/2$ the radius of cylindrical shape DRA, and H_{eff} and $\varepsilon_{r,eff}$ are the effective height and effective permittivity of the proposed antenna, respectively. H_C and H_S are

Table 1. Antenna parameters.

Symbol	Value (mm)	Symbol	Value (mm)
L_S	50	L_2	12.8
W_S	50	D	25
L_G	16.5	T	1.5
W_G	50	H_C	10
W_F	2.5	H_S	1.6
L_F	18	L_1	13

the heights of CDRA and substrate, respectively. From Eq. (1), it is clear that H_{eff} and $\varepsilon_{r,eff}$ are the most important ingredients for calculating resonant frequency of $HE_{11\delta}$ mode. These parameters are calculated as follow [1]:

$$\varepsilon_{r,eff} = \frac{H_{eff}}{\frac{H_C}{\varepsilon_{r,\text{Alumina}}} + \frac{H_S}{\varepsilon_{r,\text{sub}}}} \tag{2}$$

$$H_{eff} = H_C + H_S \tag{3}$$

There is no comprehensive formula for calculating the resonant frequency of $HE_{12\delta}$ mode. But the resonant frequency of this mode can be forecast as follow [6]:

$$f_{r,\text{HE}_{12\delta}} \geq 1.04 \times f_{r,\text{HE}_{11\delta}} \tag{4}$$

Resonant frequency for ring shape patch and inverted L-strip is calculated as follow [15]:

$$f_{\text{ring}} = \frac{X_C}{2\pi L_2\sqrt{\varepsilon_{re}}} \tag{5}$$

$$f_{\text{Inverted L-strip}} = \frac{C}{4(L_1 + L_2 + T)} \tag{6}$$

where,

$$X = \frac{2L_2}{L_2 + d} \tag{7}$$

$$\varepsilon_{re} = \frac{1}{2}(\varepsilon_{r,\text{sub}} + 1) + \frac{1}{2}(\varepsilon_{r,\text{sub}} - 1)\left(1 + \frac{10H_S}{T}\right)^{-\frac{1}{2}} \tag{8}$$

where, ε_{re} and h are effective permittivity and height of substrate, respectively; d is the outermost radius of the ring shape patch; T is the width of the ring-shaped patch. By using above formulation, the resonant frequency for $HE_{11\delta}$ and $HE_{12\delta}$ modes in CDRA are found to be 3.42 GHz and 3.66 GHz, respectively. Similarly, resonant frequencies for inverted L-strip and ring-shaped patch are found to be 2.72 GHz and 2.19 GHz, respectively.

3. ANTENNA ANALYSIS

3.1. Effect of Ground Plane on Return Loss

Figure 3 shows the return loss variation with full ground plane and various lengths of partial ground plane. It can be revealed from Fig. 3 that impedance matching of different frequency bands becomes worse with increase in the length of ground plane. It is because as the length of partial ground plane increases or with full ground plane, coupling between ground plane and ring-shaped patch increases. Due to enhancement in coupling, the ring-shaped patch is converted into ring-shaped microstrip line [16].

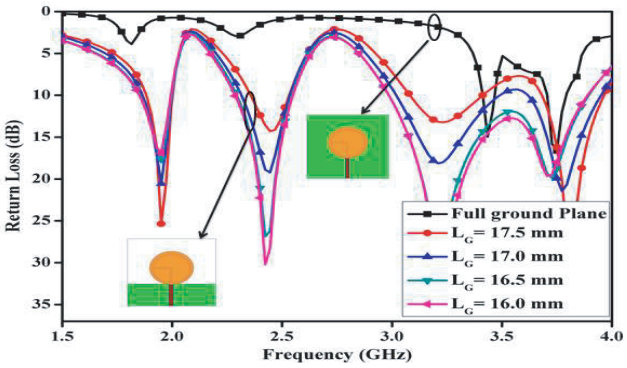

Figure 3. Return Loss variation with full ground plane and various length of partial ground plane.

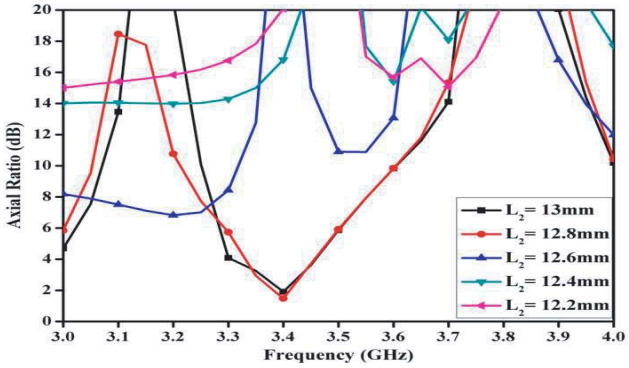

Figure 4. Axial ratio variation with various length of inverted L-strip at $\theta = 90°$ and $\varphi = 0$.

3.2. Effect of Inverted L-Strip on Axial Ratio

Figure 4 shows axial ratio variation with changing the length of inverted L-strip at $\theta = 90°$ and $\varphi = 0$. It can be observed from Fig. 4 that as the length of inverted L-strips increases, axial ratio tends towards the value of 3-dB. As the total length of L-shaped inverted strip $(L_1 + L_2)$ is 25.8 mm, the path delay becomes approximately $\frac{\lambda}{4}$ at 3.4 GHz which in turn creates the phase shift of $\frac{\pi}{2}$ between the electric field lines (phase diffference $= 2\pi/\lambda \times$ path difference). This is the reason for achieving the circular polarization characteristics.

3.3. Near Field Distribution on CDRA

Figure 5 shows near-field distributions on CDRA at 3.24 GHz and 3.75 GHz, respectively. It is clearly shown from near-field distributions that $HE_{11\delta}$-like and $HE_{12\delta}$-like modes are generated in CDRA at 3.24 GHz and 3.75 GHz, respectively [17]. High electric field of ring-shaped patch affects the horizontal E-fields in CDRA which swerves ideal orientation of $HE_{12\delta}$ mode, but radiation characteristics remain the same as $HE_{12\delta}$ mode. That is why we call it as $HE_{12\delta}$-like mode [17]. Similarly, inverted L-strip

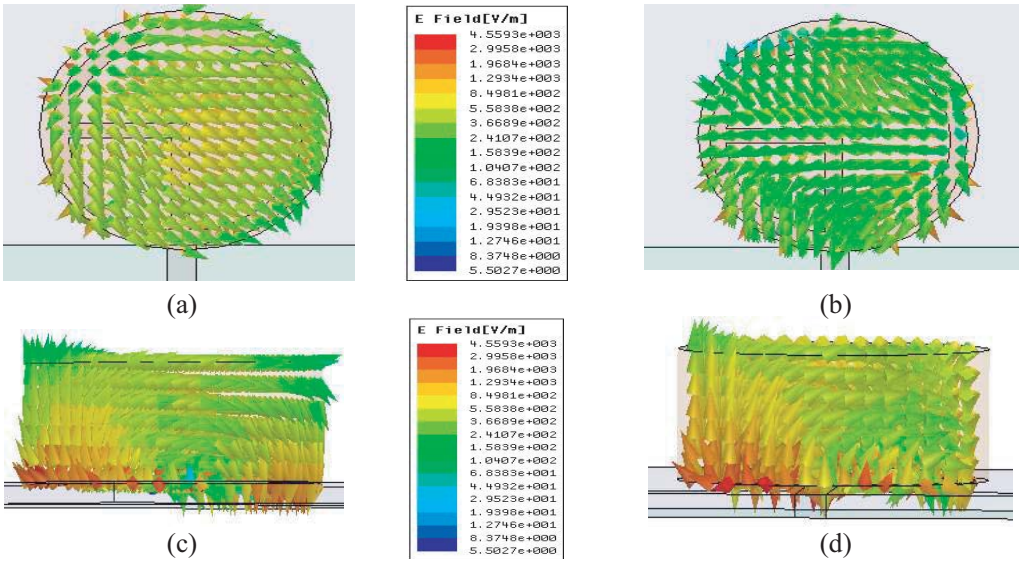

Figure 5. E-field distribution. (a) Equatorial plane at 3.24 GHz. (b) Equatorial plane at 3.75 GHz. (c) Meridian plane at 3.24 GHz. (d) Meridian plane at 3.24 GHz.

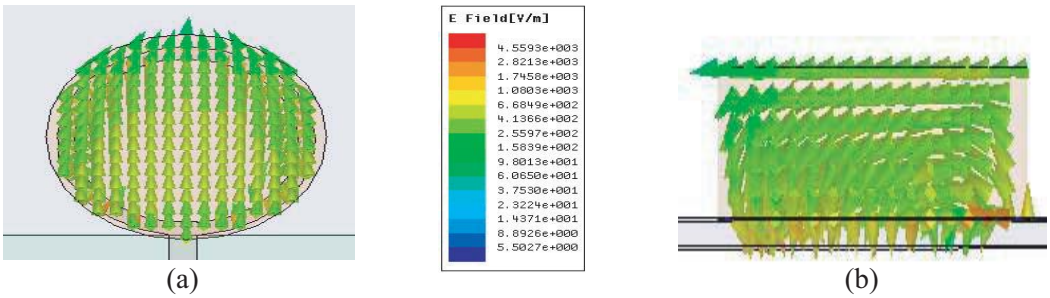

Figure 6. *E*-field distribution on CDRA without inverted L-strip. (a) Equatorial plane at 3.4 GHz. (b) Meridian plane at 3.4 GHz.

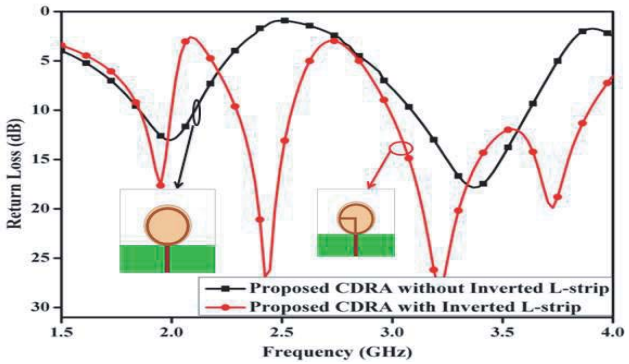

Figure 7. Return loss variation for proposed antenna design with and without inverted L-strip.

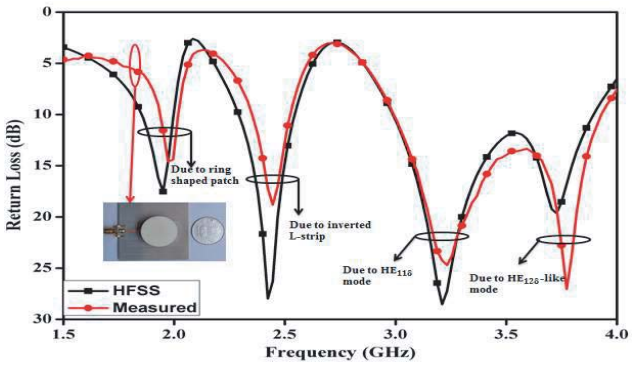

Figure 8. Measured and simulated return loss variation of proposed antenna.

creates phase shift in the ideal orientation of *E*-field of $HE_{11\delta}$ mode which is due to the path delay created by inverted L-strip. It is clearly observed by comparing the *E*-field lines of Fig. 5 and Fig. 6 (Fig. 6 shows *E*-field lines in CDRA at 3.4 GHz when there is no inverted L-strip). Therefore, we call it as $HE_{11\delta}$-like mode. Fig. 7 shows return loss variation of the proposed antenna structure with and without inverted L-strip. It can be revealed from Fig. 6 that $HE_{12\delta}$ mode in CDRA is originated due to combination of ring-shaped patch and inverted L-strip. The ring-shaped patch acts as a magnetic dipole which is in turn responsible for creation of $HE_{11\delta}$-like mode in CDRA. Similarly, the combination of ring-shaped patch and inverted L-strip acts as an electric dipole which is in turn responsible for creation of $HE_{12\delta}$ mode in CDRA [6].

4. RESULTS AND DISCUSSION

In this section, optimized simulated results are validated by using experimental results of prototype of the proposed antenna. Fig. 8 shows simulated and measured return losses of the proposed antenna, which is measured by KEYSIGHT N5221A PNA Network Analyzer (250 kHz–13.5 GHz). There is a small difference between measured and simulated results due to some of the fabrication errors such as

Table 2. Fractional bandwidth comparison of different tri-band structures.

DRA Shape	Feed Type	Lower Band (%)	Middle Band (%)	Upper Band (%)
Rectangular [4]	Microstrip Line	3.39	11.15	1.73
Cylindrical [10]	Microstrip Line	8.16	8.57	6.1
Proposed	Microstrip Line	9.13	11.9	30.16

the use of quick fix as an adhesive and the use of SMA connector whose thickness is 1.72 mm. Table 2 demonstrates the comparison of the proposed CDRA with different available DRA structures on the basis of impedance bandwidth. It can be observed from Table 2 that the proposed CDRA has larger impedance bandwidth than other existing antenna designs.

Figure 9 shows measured and simulated axial ratio variations of the proposed antenna structure at $\theta = 90°$ and $\varphi = 0$. It is measured with the help of dual-linear pattern measurement technique in the anechoic chamber [18]. Fig. 9 shows a better agreement between measured and simulated axial ratios. Measured axial ratio fractional bandwidth is approximately 7.29% (3.3–3.55 GHz). Table 3 shows comparison of the proposed antenna with other circularly polarized DRAs on the basis of axial ratio bandwidth. It is observed from Table 3 that the proposed hybrid CDRA provides larger axial ratio bandwidth.

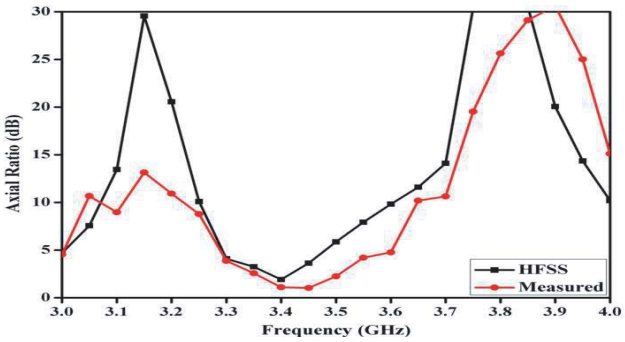

Figure 9. Measured axial ratio versus frequency graph of proposed antenna ($\theta = 90°$ and $\varphi = 0$).

Table 3. Axial ratio bandwidth comparison of proposed antenna with other existing structures.

DRA Shape	Feeding Technique	Axial Ratio Bandwidth (%)
Rectangular DRA [11]	Probe Fed	4
Semi Eccentric Annular DRA [12]	Probe Fed	5.71
Staked Rectangular [13]	Printed Line	6
Proposed CDRA	Microstrip Line	7.29

Figure 10 shows radiation pattern of the proposed antenna in E- and H-planes at 1.97 GHz, 2.44 GHz and 3.77 GHz, respectively. These radiation patterns are measured in the open environment with the help of Agilent Technologies E8275D PSG Analog Signal Generator (250 kHz–20 GHz) and ROHDE & SCHWARZ FSL Spectrum Analyzer (9 kHz–18 GHz). There is a good difference between co-polarization and cross-polarization in both the principal planes. At 3.77 GHz, the proposed antenna

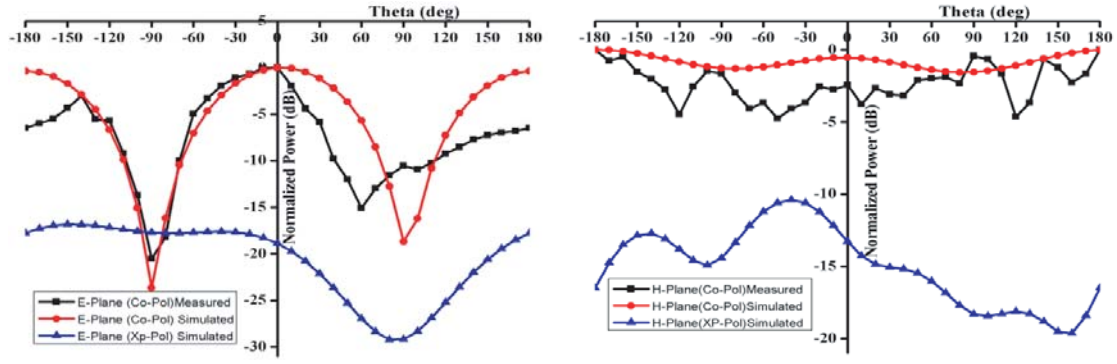

(a) (b)

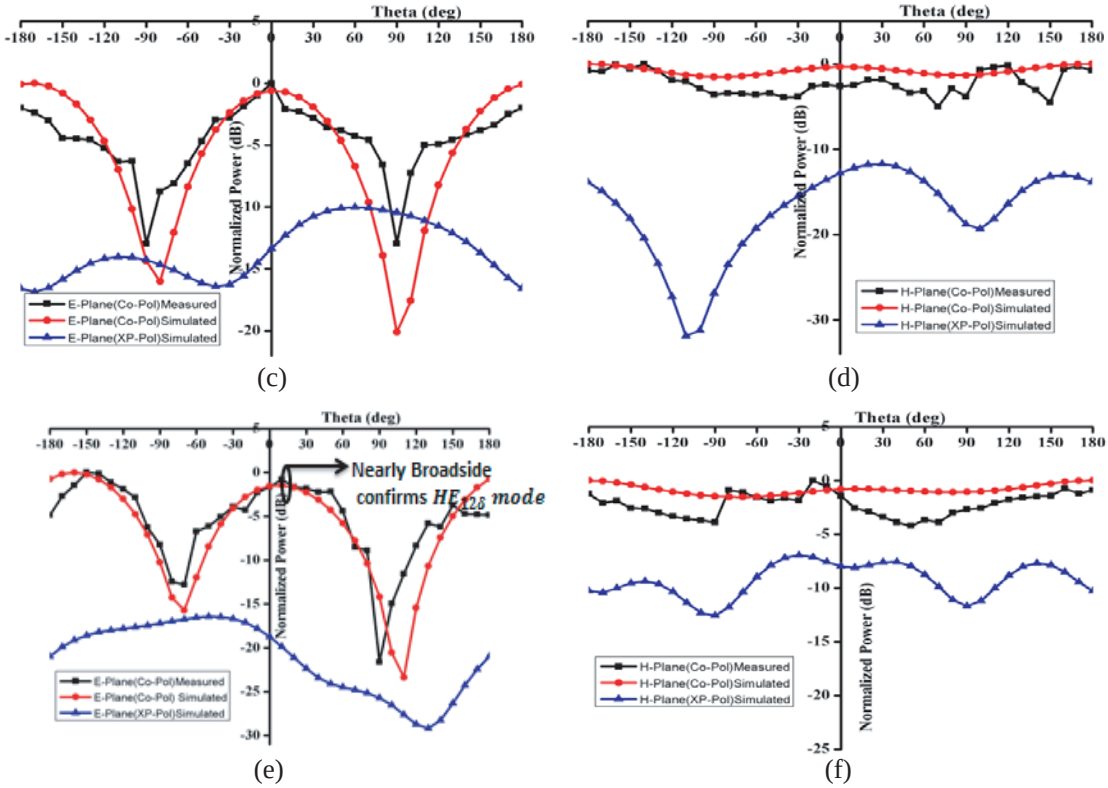

Figure 10. Far field radiation pattern of proposed antenna. (a) E-plane at 1.97 GHz. (b)H-plane at 1.97 GHz. (c) E-plane at 2.44 GHz. (d) H-plane at 2.44 GHz. (e) E-plane at 3.77 GHz. (f) H-plane at 3.77 GHz.

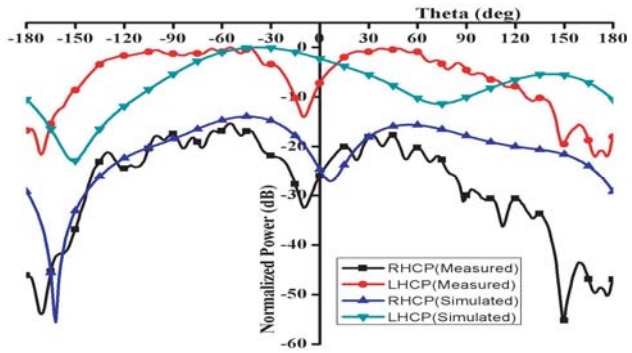

Figure 11. LHCP and RHCP at 3.4 GHz in XY-plane ($\theta = 90°$).

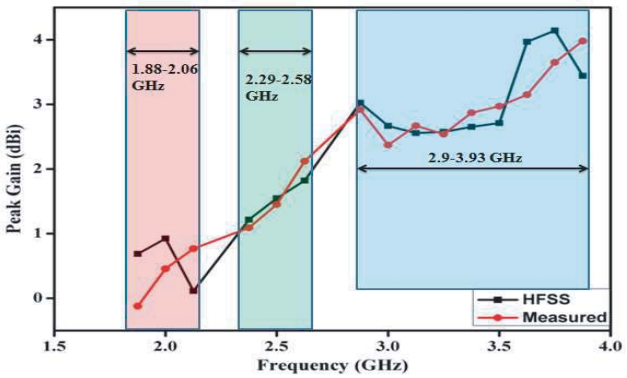

Figure 12. Measured peak gain versus frequency curve for proposed CDRA ($\theta = 0°$ and $\varphi = 0$).

radiates in the nearly broadside direction which confirms $HE_{12\delta}$-like mode in CDRA [6]. Fig. 12 shows measured and simulated LHCP and RHCP radiation patterns at 3.4 GHz (minimum axial ratio frequency) in XY-plane ($\theta = 90°$). These patterns are measured in anechoic chamber with the help of NSI SA Model 2022A antenna analyzer. It is observed from Fig. 11 that the proposed CDRA is left-handed circularly polarized because LHCP field is around 20 dB more than RHCP. Fig. 12 shows peak gain variation of the proposed antenna over the operating frequency range (shadow region in Fig. 12 where peak gain is measured). The gain is measured with the help of two antenna methods [18]. The value of peak gain is higher in between 2.9–3.93 GHz because this frequency band is originated

due to cylindrical DRA [1]. It can also be reveled from Fig. 12 that the gain of the frequency band is generated because $HE_{12\delta}$-like mode is higher than $HE_{11\delta}$ mode, and higher order mode has higher gain than fundamental mode [6].

5. CONCLUSION

In this paper, a triple-band dual-polarized hybrid cylindrical dielectric resonator antenna is presented. The main feature of the proposed article is the generation of $HE_{11\delta}$ and $HE_{12\delta}$-like modes in CDRA with the help of a modified ring-shaped patch. Both of these modes radiate in the broadside direction with possibly high amount of gain. The second important feature of the proposed antenna is the generation of triple-band characteristics with the help of hybrid antenna which makes the proposed antenna suitable for WLAN (2.4 GHz) and WiMAX (2.5/3.5 GHz) applications. The third and very important feature is the generation of circular polarization characteristics in the frequency range 3.3–3.55 GHz with the help of inverted L-strip.

ACKNOWLEDGMENT

The authors are thankful to Mr. CH Viswanathan (DGM), BEL Hyderabad, India for providing measurement facility in order to measure Axial Ratio, LHCP and RHCP measurement and also thankful to Mr. Anil Kumar Singh, Assistant Professor, MJP Rohilkhand University, Bareilly, U.P. for providing fabrication facility.

REFERENCES

1. Petosa, A., *Dielectric Resonator Antenna Handbook*, Artech House, Norwood, MA, USA, 2007.
2. Fang, X. S. and K. W. Leung, "Linear-/circular-polarization designs of dual-/wide-band cylindrical dielectric resonator antennas," *IEEE Trans. Antennas Propag.*, Vol. 60, 2662–2671, 2012.
3. Sharma, S. K. and M. K. Brar, "Aperture coupled pentagon shaped dielectric resonator antennas providing multiband and wideband performance," *Microwave Opt. Technol. Lett.*, Vol. 55, 395–400, 2013.
4. Bemani, M., S. Nikmehr and H. Younesiraad, "A novel small triple band rectangular dielectric resonator antenna for WLAN and WiMAX applications," *Journal of Electromagnetic Waves and Applications*, Vol. 25, Nos. 11–12, 1688–1698, 2012.
5. Guha, D., H. Gajera, and C. Kumar, "Cross-polarized radiation in a cylindrical dielectric resonator antenna: Identification of source, experimental proof, and its suppression," *IEEE Trans. Antennas Propag.*, Vol. 63, 1863–1867, 2015.
6. Guha, D., A. Banerjee, C. Kumar, and Y. M. M. Antar, "Higher order mode excitation for high-gain broadside radiation from cylindrical dielectric resonators antennas," *IEEE Trans. Antennas Propag.*, Vol. 60, 71–77, 2012.
7. Lin, Y.-F., H.-M. Chen, and C.-H. Lin, "Compact dual-band hybrid dielectric resonator antenna with radiating slot," *IEEE Antennas and Wireless Propag. Lett.*, Vol. 8, 6–9, 2009.
8. Ding, Y. and K. W. Leung, "On the dual-band DRA-slot hybrid antenna," *IEEE Trans. Antennas Propag.*, Vol. 57, 624–630, 2009.
9. Khalily, M., M. K. A. Rahim, and M. R. Kamarudin, "Modified cylindrical dielectric resonators excited with loaded fork monopole antenna," *Microwave Opt. Technol. Lett.*, Vol. 53, 2887–2890, 2011.
10. Sharma, A. and R. K. Gangwar, "Compact tri-band cylindrical dielectric resonator antenna with circular slots for wireless application," *Journal of Electromagnetic Waves and Applications,* Vol. 30, No. 3, 331–340, 2016.
11. Fang, X., K. W. Leung, and E. H. Lim, "Singly-fed dual-band circularly polarized dielectric resonator antenna," *IEEE Antennas and Wireless Propag. Lett.*, Vol. 13, 532–535, 2014.

12. Lee, J. M., S. J. Kim, G. Kwon, C. M. Song, Y. Yang, K. Y. Lee, and K. C. Hwang, "Circularly polarized semi eccentric annular dielectric resonator antenna for X-band applications," *IEEE Antennas and Wireless Propag. Lett.*, Vol. 14, 1810–1813, 2015.
13. Khalily, M., M. R. Kamarudin, M. Mokayef, and M. H. Jamaluddin, "Omnidirectional circularly polarized dielectric resonator antenna for 5.2 GHz WLAN-applications," *IEEE Antennas and Wireless Propag. Lett.*, Vol. 13, 443–446, 2014.
14. Mongia, R. K. and P. Bhartia, "Dielectric resonator antennas-a review and general design relations for resonant frequency and bandwidth," *International Journal of Microwave and Millimeter-wave Computer Aided Engineering*, Vol. 4, 230–247, 1994.
15. Garg, R., P. Bhartia, I. Bahl and A. Ittipiboon, *Microstrip Antenna Design Handbook*, Artech House, Norwood, MA, USA, 2001.
16. Best, S. R., "The significance of ground-plane size and antenna location in establishing the performance of ground-plane-dependent antennas," *IEEE Antennas and Propag. Magazine*, Vol. 51, 29–43, 2009.
17. Kajfez, D., A. W. Glisson, and J. James, "Computed modal field distributions for isolated dielectric resonators," *IEEE Trans. Microwave Theory and Techniques*, Vol. 32, 1609–1616, 1984.
18. Balanis, C. A., *Antenna Theory: Analysis and Design*, A John Wiley & Sons, INC., Publication, 2005.